Self-Connected and Habitually Tilted Piezoelectric Nanorod Array

Hak Ki Yu,[†] Jeong Min Baik,[‡] and Jong-Lam Lee[†,*]

[†]Division of Advanced Materials Science and Department of Materials Science and Engineering, Pohang University of Science and Technology (POSTECH), Pohang, 790-784, Korea and, [‡]School of Mechanical and Advanced Materials Engineering, Ulsan National Institute of Science & Technology (UNIST), Ulsan, 689-805, Korea

ABSTRACT

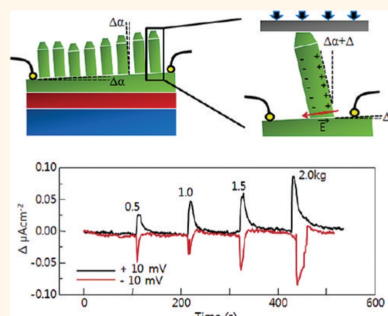

We fabricated a self-connected and habitually tilted ZnO nanorod (NR) array, which is free of any patterning process for the connection of the NRs and is easily bent by a normal force. The vertically well-aligned ZnO NRs were grown by a strain relaxation process on MgO-buffered C-plane sapphire, and the remaining epitaxial ZnO wetting layer acted as a self-connecting layer of NRs. The epitaxial ZnO film on the step-terrace structured substrate caused the tilting angle from the surface normal direction (~0.2°) to match the step between the ZnO film and MgO-buffered C-plane sapphire, resulting in easy bending of the ZnO NRs by normal force. The unsymmetrical strain between the tensile and compressive stressed region in the habitually tilted ZnO NRs caused a gradient in the piezoelectric potential, resulting in an electrical field along the lateral direction of NR growth, resulting in the control of the current direction and level to be about 0.1 μA/cm^2 at 2 kgf normal force.

KEYWORDS: ZnO · nanorod · piezoelectricity · habitual tilting · self-connected

Piezoelectric ZnO nanorods (NRs) that are both well aligned and bent in specific directions by external forces could have potential applications in piezotronic devices, such as field effect transistors, energy harvesting, and pressure sensing devices.[1−5] Generally, in many piezoelectric devices, vertically arranged electrodes (top and bottom) were used due to the randomly tilted NRs by the external force.[6,7] However, the vertical electrodes have problems with their fabrication process; the bottom electrode affects the NR growth mode, such as the density, size, and orientation.[8] Moreover, it is difficult to make a top electrode on NRs owing to sidewall deposition. In some cases, the bending of ZnO NRs was prohibited by the sidewall passivation process.[9] To solve these problems, laterally aligned ZnO NRs were used by using the sweeping-printing method and lateral-growth method. However, the patterning process for the lateral electrode was also needed, and the substrate needed to be flexible for the bending torque.[9,10]

In this study, we fabricated a self-connected and habitually tilted ZnO NRs array, which is free of any patterning process for the connection of NRs and is easily bent by a simple normal force. We used MgO as a buffer layer for the epitaxial growth of ZnO on C-plane sapphire (Figure 1a). The vertically well aligned ZnO NRs were grown by a strain relaxation process, and the remaining epitaxial wetting layer acted as a self-connecting layer of NRs, as shown in Figure 1b. The habitual tilting angle ($\Delta\alpha$ in Figure 1c) was achieved by epitaxial ZnO film growth on a step-terrace structure to match the step by introducing a tilt between films.[11−13] The self-connected and well-aligned ZnO NRs were tilted from the surface normal direction due to the epitaxial tilted wetting layer, resulting in easy bending by the normal force. The unsymmetrical strain between the tensile and compressive stressed region in the tilted ZnO NRs caused a gradient in the piezoelectric potential, resulting in an electrical field along the lateral direction of NR growth, as shown in Figure 1c.[14−16] By using the electrical field formed in each NR, we could control the direction and level of the passing current easily. Moreover, the large scale application is also possible by connecting several devices in series without transfer of ZnO NRs. These results suggest an experimental approach to the simplest fabrication method for future piezoelectric devices.

RESULTS AND DISCUSSION

The lattice mismatch between MgO (111) and C-plane sapphire is about 8.4% and that

* Address correspondence to jllee@postech.ac.kr.

Received for review August 1, 2011 and accepted October 20, 2011.

Published online October 20, 2011
10.1021/nn202985q

© 2011 American Chemical Society

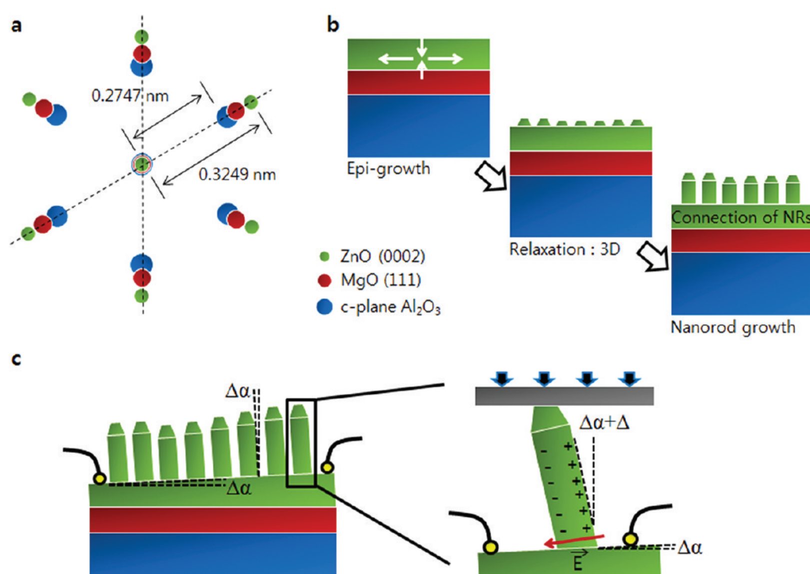

Figure 1. (a) Atomic configuration in the ZnO/MgO/C−Al_2O_3 system with epitaxial relationship followed by (0001)-$[1\bar{2}10]_{ZnO}$|| (111) $[1\bar{1}0]_{MgO}$|| (0001) $[1\bar{1}00]_{C\text{-sapphire}}$. The lattice mismatch between ZnO and C-plane sapphire could be reduced by using MgO buffer layer. (b) Steps for ZnO NR growth: epitaxial growth; strain relaxation (roughened surface); NR growth with C-preferred orientation. (c) Schematic view of self-connected and habitually tilted ZnO NR (Δα) array and device application for the piezoelectric application. The additional tilt (Δ) causes unsymmetrical strain in ZnO NR, resulting in a lateral electric field.

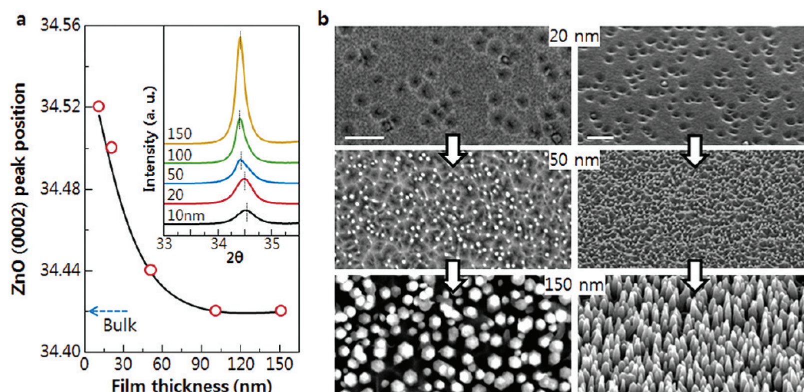

Figure 2. (a) XRD radial scans ($\theta-2\theta$) along the surface normal for the ZnO films on MgO-buffered sapphire (film thicknesses from 10 to 150 nm). No impurity or polycrystalline ZnO peaks were detected except for the epitaxial ZnO (0002). The peak position was shifted to lower 2θ angles as the film thickened and saturated above the 100 nm region. The inset shows the (0002) ZnO peak-position by using Gaussian fitting. The bulk (0002) peak position is 34.32°. (b) Top and 3D view SEM images of the ZnO film surface grown on MgO-buffered sapphire (20, 50, and 150 nm). Scale bar, 200 nm.

of ZnO (0002) on MgO (111) is about 9%. Generally, lattice matching epitaxy is almost impossible if the lattice mismatch is more than 7%.[17,18] However, in systems with a large lattice mismatch, epitaxial growth of thin films is made possible by matching domains where integral multiples of major lattice planes match across the interface.[19,20] In the epitaxial system of ZnO/MgO/C-plane sapphire defined as (0001) $[1\bar{2}10]_{ZnO}$||-(111) $[1\bar{1}0]_{MgO}$|| (0001) $[1\bar{1}00]_{C\text{-sapphire}}$, the 11/12/13 domain matching has the lowest domain mismatch value, and this calculation was confirmed by HR-TEM micrographs and its Fourier filtered images (Supporting Information Table S1 and Figures S1, S2, and S3). The epitaxial ZnO (0002) film on the MgO (111)-buffered C-plane sapphire had a larger 2θ position than the bulk state for thin films with thicknesses smaller than 50 nm due to the smaller domain size of ZnO (3.5739 nm) compared to MgO (3.5748 nm) in the 11/12 domain matching structure, resulting in tensile strain at the in-plane direction and compressive strain at the out-of-plane direction. The applied strain of the ZnO film was relaxed above 50 nm film thicknesses and the (0002) peak approached the bulk value (Figure 2a). During strain relaxation, the surface morphology drastically changed from a 2D flat surface (20 nm) to 3D nanostructures (150 nm) (Figure 2b). The remained ZnO wetting layer at the bottom of all ZnO NRs has enough Hall mobility and carrier (electron) concentration (Supporting Information Table S1) to be used as bottom electrode due to natural oxygen vacancies and zinc interstitials.

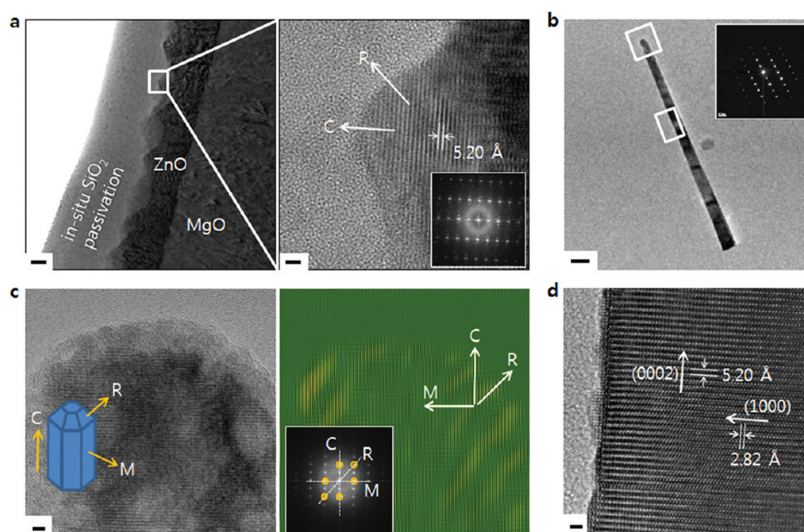

Figure 3. (a) Cross-sectional TEM image of the sample ZnO (50 nm) on MgO-buffered sapphire. To analyze the surface morphology after strain relaxation, the sample was *in situ* deposited by using amorphous SiO_2. Scale bar, 20 nm. The enlarged HR-TEM image shows the specific crystal termination of the roughened ZnO surface after strain relaxation, C and R. Scale bar, 2 nm. (b) TEM image of single and C-oriented ZnO NR. The length of the NR is about 1.2 μm. Scale bar, 100 nm. (c) HR-TEM image of the ZnO NR head in Figure 3b and schematic view of pencil-type ZnO NR with C, R, and M termination. Scale bar, 2 nm. Fourier filtered image is also shown by masking C, R, and M orientation of ZnO. (d) HR-TEM image of the body of ZnO NR in Figure 3b with termination of M (1000). Scale bar, 1 nm.

At the early stage of relaxation (50 nm thicknesses), the C-oriented ZnO (0002) film exhibited a specific 3D nanostructure with nonpolar R-(1$\bar{1}$02) termination after strain relaxation (Figure 3a). In the viewpoint of polarity, the C-oriented ZnO with alternating Zn cation and O anion layers has strong polarity, and it has the largest number of dangling bonds per atom on the topmost surface due to the same atomic array existing in one monolayer.[21−23] A lot of dangling bonds are needed to be energetically stabilized by dominantly adsorbing adatoms, resulting in C-oriented ZnO nanostructures after strain relaxation.[24,25] The 1.2 μm length of C-oriented ZnO NRs (Figure 3b) were grown without any catalyst, and the surfaces of the head were terminated by the nonpolar (1$\bar{1}$02) R-orientation as shown in the HR-TEM micrograph, resulting in a pencil shape (Figure 3c). The clear orientation of the pencil type ZnO NRs also could be shown by a Fourier filtering image. This was done by masking C, M, and R orientations of a Fourier transformed pattern with reciprocal spacings of 3.842, 3.554, and 5.233 nm^{-1}, respectively. The body of the ZnO NR was atomically well aligned with a lattice spacing of 0.520 nm and terminated by nonpolar (10$\bar{1}$0) M-orientation with a lattice spacing of 0.282 nm (Figure 3d). The most important parameter to determine the spacing of ZnO NR is the strain between adequate buffer layer and ZnO. Although we used the MgO layer as a buffer in this experiment, any kinds of buffer layer which has close packed crystal structure such as rock-salt, wurtzite, and corundum is possible for the epitaxial ZnO growth. For instance, rock-salt crystal such as NiO (inter-atomic distance is 0.295 nm), TiN (0.3 nm), CoO (0.301 nm), and TaN (0.306 nm) is possible. Moreover, wurtzite crystal such as GaN (0.3186 nm) is also possible for the buffer layer. As the accumulated strain increases with respect to buffer layer material, the strain relaxation could happen earlier, resulting in high density of NRs. The size of NRs could be affected by growth time after strain relaxation. Although a lot of adatoms strongly tend to stick on the C-plane of ZnO, the growth of the R-plane is also preceded. So, the diameter of ZnO NRs increased as growth time increased after strain relaxation as shown in Supporting Information Figure S4.

The surface of the bare C-plane sapphire annealed at 1000 °C in atmosphere had a natural step-terrace structure, as shown in Figure 4a, and the epitaxially grown MgO film (10 nm) also followed the step-terrace shape. In the 11/12 domain matching system of ZnO/MgO, the habitually tilted ZnO film could be theoretically acquired, as shown in Figure 4b. For a step-terrace angle (α) of a domain-matched MgO buffer layer, the step matching requirement introduces a tilt between the ZnO film and the MgO buffer layer, $\Delta\alpha$, given by[11]

$$\Delta\alpha = \tan^{-1}\left(\frac{d_s - d_f}{d_s}\tan\alpha\right)$$

, where d_s and d_f are the d-spacing of substrate and film, respectively. For the 11/12 (ZnO/MgO) domain matching system, the detailed spatial tilt could be calculated to be 0.27°; d_s is 0.243 nm, d_f is 0.260 nm, and tan α is 0.243 nm/3.5748 nm (terrace length of 12 MgO lattice) in this case. In the XRD RSM patterns from C-plane sapphire to ZnO (Figure 4c), the ZnO grown on bare sapphire had coherent surface normal

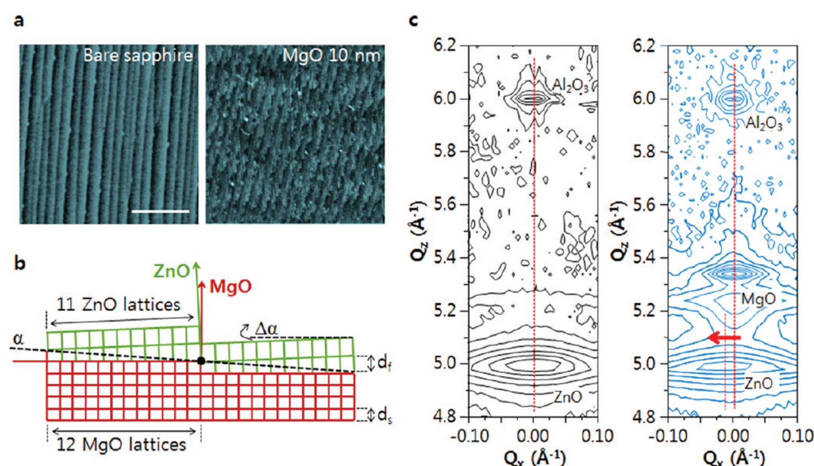

Figure 4. (a) AFM images of bare C-plane sapphire and MgO deposited (10 nm) sapphire surfaces. Scale bar, 200 nm. (b) Schematic view of 11/12 domain matched ZnO/MgO interface with step-terrace structure. Tilting of ZnO film (Δα) for the lattice matching at the step-terrace region of MgO with α angle. The d_f and d_s are the *d*-spacing of film and substrate, respectively. (c) XRD-RSM images around C−Al_2O_3 reflections for bare ZnO film and MgO-buffered ZnO film.

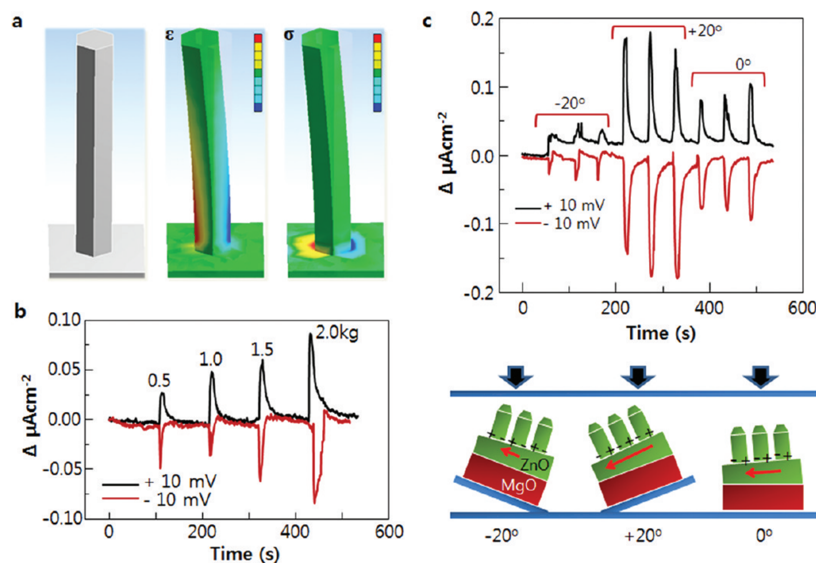

Figure 5. (a) The strain (ε) and stress (σ) simulation results of ZnO NR grown on a ZnO wetting layer plate using the finite element method. The red zone in strain and stress map is the compressive region, and the blue one is the tensile region. The applied force was 2 kgf and the vector direction was tilted 20° from the surface normal. (b) Change of the current with respect to applied force at the constant voltage of ±10 mV. (c) Additional change in current by placing the sample on a different slope at the constant voltage of ±10 mV (normal, +20°, and −20°). The schematic sketches show the electric field with respect to slope angle for the case of +10 mV.

characteristics, whereas that on MgO-buffered C-plane sapphire tilted away about 0.2° from the surface normal direction; the angle could be calculated as[26]

$$\tan^{-1}(\Delta Q_x/Q_z) = \tan^{-1}(0.0172/4.98)$$

and this result agrees well with the previous Δα calculation. Because the habitual tilting angle was so small (measured about 0.2°), it is difficult to see the exact tilting angle directly by 3D SEM images in Figure 2b.

Habitual tilt of ZnO NRs caused an unsymmetrical strain distribution due to the bending of NRs by the horizontally projected normal force. Specifically, the strain gradient was dominant at the bottom area of the NRs and the stress was dominantly distributed at the interface of the 2D wetting layer and NRs (Figure 5a). In the tensile strained region of the ZnO NRs, the piezoelectric potential is positive, whereas it is negative in the compressive strained region. The gradient of the piezoelectric potential near the bottom of the NRs resulted in an electrical field along the lateral direction of the NR growth, and this could be used in piezoelectric device applications.[14−16] The electric field direction in ZnO NRs by external force could be the same or opposite with respect to the applied voltage of ±10 mV because the ZnO NRs were tilted in specific

directions. The change of the current density increased linearly as the external force increased from 0.5 to 2 kgf for the ZnO NRs on MgO-buffered C-sapphire (Figure 5b). However, randomly distributed ZnO NRs have a nonlinear relationship between applied force and their current density change (Supporting Information Figure S5). The change of current density could also increase by leveling a tilting angle. Figure 5c shows the change of the current density at the constant ±10 mV and 2 kgf external forces by modulating the tilt angle. Habitual tilted ZnO NRs were placed at 20° and −20° slopes, respectively. If the slope is the same direction as the habitual tilted angle of ZnO, the change of the current density increased by about 2 times compared with the normal slope. On the other hand, the change of current density decreased about 2 times when the slope angle is reversed with the habitual tiled angle of the ZnO NRs. From these *I*−*V* measurements, we could know that ZnO NRs were spatially tilted in one direction by the MgO buffer layer.

CONCLUSION

In summary, this letter has provided the first demonstration of the self-connected and habitually tilted ZnO NRs array using an epitaxial wetting layer and step matching method. The ZnO NRs array causes an unsymmetrical piezoelectric field direction by external force due to habitual tilting, resulting in the control of the current direction and level at about 0.1 μA/cm^2 at 2 kgf normal force. The change of the current level by external force also could be controlled by using a tilting substrate *via* adjusting additional torque on the ZnO NR array. As it is the first demonstration of a self-connected and habitually tilted ZnO NR array, this result suggests the simplest fabrication method for future piezoelectric devices.

METHODS

A self-connected and habitually tilted ZnO NR array was fabricated on MgO-buffered C-sapphire using an electron beam evaporation method. A C-plane sapphire was used as a starting substrate. The substrate was cleaned sequentially with acetone, ethyl-alcohol, and deionized water. Before MgO/ZnO film deposition, the C-sapphire substrate was annealed at 1000 °C in atmosphere to form clear step-terrace structure. MgO films were deposited using high purity MgO pellets made by compressing and heating 99.995% MgO powder (Mitsubishi Materials Co.). MgO films were grown to 10 nm thicknesses at a rate of 0.1 nm s^{-1}. The chamber pressure was maintained at about 10^{-6} Torr during deposition and the substrate temperature was held at 400 °C. *In-situ* ZnO deposition followed using high purity ZnO pellets (99.99% with a diameter of 3 mm). The ZnO was grown to 150 nm thickness at a rate of 0.1 nm s^{-1} at a substrate temperature of 600 °C. High-resolution XRD using synchrotron radiation was performed at the 3C2 beamline at the Pohang Accelerator Laboratory. For high-resolution XRD measurements, the wavelength of the incident X-ray was set at 1.488 Å using a double bounce Si (111) monochromator. Atomic force microscopy (AFM) images were recorded using a Digital Instruments Nanoscope in tapping mode using silicon cantilevers. SEM was done using a PHILIPS XL30S with an accelerating voltage of 10 kV and a working distance of 5 mm. The HR-TEM images were collected using a Cs-corrected JEM 2200FS operated at 200 kV.

The piezoelectric devices were fabricated as described below. After the ZnO NR growth, laterally arranged electrodes were formed by indium wire bonding. The external force was applied by pushing the insulating glass block put on the ZnO NR arrays. Exact values of applied force were measured by using an electronic scale. The *I*−*V* changes with respect to applied force were measured under air ambient using a Keithley 2400 source measurement unit. The bending of ZnO was simulated by the finite element method using an Ansys program version 13.0. The hexagonal ZnO NR with 100 nm diameter and 1 μm length was put on the ZnO plate. The fixed plane in our calculation is the bottom of the ZnO plate. The applied force in the ZnO NR was divided into vertical and horizontal elements using trigonometric functions. The mechanical properties of ZnO such as elastic modulus, Poisson's ratio, ultimate strength, and yield strength were acquired from the references.[27−29]

Acknowledgment. This study was supported in part by Priority Research Centers Program through the National Research Foundation of Korea (NRF) funded by the Ministry of Education, Science and Technology (2010-0029711) and in part by a WCU (World Class University) program through the Korea Science and Engineering Foundation funded by the Ministry of Education, Science and Technology (Project No. R31-2008-000-10059-0).

Supporting Information Available: Additional figures and tables as described in the text. This material is available free of charge *via* the Internet at http://pubs.acs.org.

REFERENCES AND NOTES

1. Qin, Y.; Wang, X.; Wang, Z. L. Microfiber−Nanowire Hybrid Structure for Energy Scavenging. *Nature* **2008**, *451*, 809–813.
2. Park, H.-K.; Lee, K. Y.; Seo, J.-S.; Jeong, J.-A.; Kim, H.-K.; Choi, D.; Kim, S.-W. Charge-Generating Mode Control in High-Performance Transparent Flexible Piezoelectric Nanogenerators. *Adv. Funct. Mater.* **2011**, *21*, 1187–1193.
3. Wang, X.; Zhou, J.; Song, J.; Liu, J.; Xu, N.; Wang, Z. L. Piezoelectric Field Effect Transistor and Nanoforce Sensor Based on a Single ZnO Nanowire. *Nano Lett.* **2006**, *6*, 2768–2772.
4. Zhou, J.; Gu, Y.; Fei, P.; Mai, W.; Gao, Y.; Yang, R.; Bao, G.; Wang, Z. L. Flexible Piezotronic Strain Sensor. *Nano Lett.* **2008**, *8*, 3035–3040.
5. Wang, Z. L. Nanopiezotronics. *Adv. Mater.* **2007**, *19*, 889–892.
6. Wang, X.; Song, J.; Liu, J.; Wang, Z. L. Direct-Current Nanogenerator Driven by Ultrasonic Waves. *Science* **2007**, *316*, 102–105.
7. Choi, M.-Y.; Choi, D.; Jin, M.-J.; Kim, I.; Kim, S.-H.; Choi, J.-Y.; Lee, S. Y.; Kim, J. M.; Kim, S. W. Mechanically Powered Transparent Flexible Charge-Generating Nanodevices with Piezoelectric ZnO Nanorods. *Adv. Mater.* **2009**, *21*, 2185–2189.
8. Choy, J.-H.; Jang, E.-S.; Won, J.-H.; Chung, J.-H.; Jang, D.-J.; Kim, Y.-W. Soft Solution Route to Directionally Grown ZnO Nanorod Arrays on Si Wafer; Room-Temperature Ultraviolet Laser. *Adv. Mater.* **2003**, *15*, 1911–1914.
9. Xu, S.; Qin, Y.; Xu, C.; Wei, Y.; Yang, R.; Wang, Z. L. Self-Powered Nanowire Devices. *Nat. Nanotechnol.* **2010**, *5*, 366–373.
10. Zhu, G.; Yang, R.; Wang, S.; Wang, Z. L. Flexible High-Output Nanogenerator Based on Lateral ZnO Nanowire Array. *Nano Lett.* **2010**, *10*, 3151–3155.
11. Budai, J. D.; Yang, W.; Tamura, N.; Chung, J.-S.; Tischler, J. Z.; Larson, B. C.; Ice, G. E.; Park, C.; Norton, D. P. X-ray

Microdiffraction Study of Growth Modes and Crystallographic Tilts in Oxide Films on Metal Substrates. *Nat. Mater.* **2003**, *2*, 487–492.
12. Nagai, H. Structure of Vapor-Deposited $Ga_xIn_{1-x}As$ Crystals. *J. Appl. Phys.* **1974**, *45*, 3789–3794.
13. Ayers, J. E.; Ghandhi, S. K.; Schowalter, L. J. Crystallographic Tilting of Heteroepitaxial Layers. *J. Cryst. Growth* **1991**, *113*, 430–440.
14. Chung, K. W.; Wang, Z.; Costa, J. C.; Williamson, F.; Ruden, P. P.; Nathan, M. I. Barrier Height Change in GaAs Schottky Diodes Induced by Piezoelectric Effect. *Appl. Phys. Lett.* **1991**, *59*, 1191–1193.
15. Zhou, J.; Fei, P.; Gu, Y.; Mai, W.; Gao, Y.; Yang, R.; Bao, G.; Wang, Z. L. Piezoelectric-Potential-Controlled Polarity-Reversible Schottky Diodes and Switches of ZnO Wires. *Nano Lett.* **2008**, *8*, 3973–3977.
16. Zhao, M.-H. ; Wang, Z. L.; Mao, S. X. Piezoelectric Characterization on Individual Zinc Oxide Nanobelt under Piezoresponse Force Microscope. *Nano Lett.* **2004**, *4*, 587–590.
17. Matthews, J. W.; Blakeslee, A. E. Defects in Epitaxial Multilayers: I. Misfit Dislocations. *J. Cryst. Growth* **1974**, *27*, 118–125.
18. Freund, L. B.; Nix, W. D. A Critical Thickness Condition for a Strained Compliant Substrate/Epitaxial Film System. *Appl. Phys. Lett.* **1996**, *69*, 173–175.
19. Yu, H. K.; Baik, J. M.; Lee, J.-L. Design of an Interfacial Layer to Block Chemical Reaction for Epitaxial ZnO Growth on a Si Substrate. *Cryst. Growth Des.* **2011**, *11*, 2438–2443.
20. Yu, H. K.; Lee, J.-L. Growth Mechanism of MgO Film on Si (100): Domain Matching Epitaxy, Strain Relaxation, Preferred Orientation Formation. *Cryst. Growth Des.* **2010**, *10*, 5200–5204.
21. Wolf, D. Reconstruction of NaCl Surfaces from a Dipolar Solution to the Madelung Problem. *Phys. Rev. Lett.* **1992**, *68*, 3315–3318.
22. Noguera, C. Polar Oxide Surfaces. *J. Phys.: Condens. Matter* **2000**, *12*, R367–R410.
23. Kong, X. Y.; Ding, Y.; Yang, R.; Wang, Z. L. Single-Crystal Nanorings Formed by Epitaxial Self-Coiling of Polar Nanobelts. *Science* **2004**, *303*, 1348–1351.
24. Greene, J. E.; Sundgren, J.-E.; Hultman, L.; Petrov, I.; Bergstrom, D. B. Development of Preferred Orientation in Polycrystalline TiN Layers Grown by Ultrahigh Vacuum Reactive Magnetron Sputtering. *Appl. Phys. Lett.* **1995**, *67*, 2928–2930.
25. Liu, X.-Y. ; Bennema, P. Theoretical Consideration of the Growth Morphology of Crystals. *Phys. Rev. B* **1996**, *53*, 2314–2325.
26. Jang, H. W.; Ortiz, D.; Baek, S.-H.; Folkman, C. M.; Das, R. R.; Shafer, P.; Chen, Y.; Nelson, C. T.; Pan, X.; Ramesh, R.; *et al.* Domain Engineering for Enhanced Ferroelectric Properties of Epitaxial (001) BiFeO Thin Films. *Adv. Mater.* **2009**, *21*, 817–823.
27. Riaz, M.; Fulati, A.; Zhao, Q. X.; Nur, O.; Willander, M.; Klason, P. Buckling and Mechanical Instability of ZnO Nanorods Grown on Different Substrates under Uniaxial Compression. *Nanotechnology* **2008**, *19*, 415708.
28. Kulkarni, A. J.; Zhou, M.; Ke, F. J. Orientation and Size Dependence of the Elastic Properties of Zinc Oxide Nanobelts. *Nanotechnology* **2005**, *16*, 2749–2756.
29. Catti, M.; Noel, Y.; Dovesi, R. Full Piezoelectric Tensors of Wurtzite and Zinc Blende ZnO and ZnS by First-Principles Calculations. *J. Phys. Chem. Solids* **2003**, *64*, 2183–2190.